Determination of the Rate Constants for the Radical−Radical Reactions $NH_2(\tilde{X}^2B_1)$ + $NH(X^3\Sigma^-)$ and $NH_2(\tilde{X}^2B_1)$ + $H(^2S)$ at 293 K

Mi-Kyung Bahng[†] and R. Glen Macdonald*

Chemical Sciences and Engineering Division, Argonne National Laboratory, 9700 South Cass Avenue, Argonne, Illinois 60439-4831

Received: October 31, 2008; Revised Manuscript Received: January 7, 2009

The rate constant for the reactions $NH_2(\tilde{X}^2B_1)$ + $NH(X^3\Sigma^-)$ and $NH_2(\tilde{X}^2B_1)$ + $H(^2S)$ were measured over a pressure range from 2 to 10 Torr in CF_4, or Ar gases at 293 ± 2 K. The radicals were produced by the 193 nm photolysis of NH_3 dilute in the carrier gas. Both radicals were monitored simultaneously following the photolysis laser pulse using high-resolution time-resolved absorption spectroscopy. The NH_2 radical was monitored using the $^12_{21} \leftarrow {}^13_{31}$ rotational transition of the $(0,7,0)\tilde{A}^2A_1 \leftarrow (0,0,0)\ \tilde{X}^2B_1$ vibronic band near 675 nm, and the NH radical was monitored using the $^1R_3(4)$ rotational transition on the 1−0 vibrational transition near 3084 nm. The data was analyzed using model simulations of the NH_2 and NH temporal concentration profiles. The rate constants for the NH_2 + NH and NH_2 + H reactions were found to be $(9.6 \pm 3.2) \times 10^{-11}$ and $(7.7 \pm 14) \times 10^{-15}$ cm^3 $molecule^{-1}$ s^{-1}, respectively, where the uncertainty includes an estimate of both systematic and random errors. The measurements were independent of the nature of the diluents, CF_4 or Ar, and total pressure.

1. Introduction

Radical−radical reactions are a unique class of chemical reactions.[1] The interaction of two species with unpaired electron spin always involves multiple potential energy surfaces (PESs) because of the parallel and antiparallel alignment of the electron spin. If one of the interacting radicals also possesses electronic angular momentum, then there are also multiple electronic as well as spin manifolds. The antiparallel arrangement of electron spin, corresponding to a bonding interaction, usually results in an attractive PES. The bond energy in the newly forming bond is available to the new molecule, and can be redistributed through out the chemically activated complex. If there are weaker bonds in the complex, these can undergo fragmentation. Thus, radical−radical reactions generally have the possibility of multiple product channels from both addition elimination mechanisms and the presence of multiple PESs.[2] Because of this complex chemistry, radical−radical reactions are an important class of chemical reactions in combustion chemistry and other environments as they are chain terminating, and/or chain propagating steps leading to new chemical species and more complex chemistry.

Reactions involving N_iH_j radicals are an excellent example of the complex chemistry occurring in radical−radical interactions. These species play an important role in the pyrolysis and combustion chemistry of NH_3 as well as other combustion environments.[3,4] Furthermore, the radicals imidogen, $NH(X^3\Sigma^-)$, and amidogen, $NH_2(\tilde{X}^2B_1)$, are unique because they can react with $NO(X^2\Pi)$ to produce N_2O and N_2, converting an undesirable pollutant into mostly benign byproduct. Several flue gas treatments for reduction of NO_X from stationary sources take advantage of these reactions. The Thermal deNO_X process is based on the direct addition of NH_3 to combustion flue gases. Other flue gas treatments are based on the addition of urea or cyanuric acid generating these radicals and removing NO from the gas stream.[3] Although NH and NH_2 radicals play an important role in combustion chemistry, many of the reactions involving these radicals especially with other N_iH_j radicals have not been extensively investigated.[5] This is especially true at lower temperatures. The radical−radical reaction NH + NH_2 is an interesting case study of one of these N_iH_j radical−radical reactions.

In the present work, the rate constants for reactions 2a, k_{2a}

$$NH_2(\tilde{X}^2B_1) + H(^2S) \rightarrow NH(^3\Sigma^-) + H_2 \qquad (2a)$$

and reaction 3, $k_3 = k_{3a} + k_{3b} + k_{3c}$

$$NH_2(\tilde{X}^2B_1) + NH(X^3\Sigma^-) \rightarrow NH_3 + N(^4S_u) \qquad (3a)$$

$$\rightarrow N_2H_2 + H(^2S) \qquad (3b)$$

$$NH_2(\tilde{X}^2B_1) + NH(X^3\Sigma^-) + M \rightarrow N_2H_3(\tilde{X}^2A') + M \qquad (3c)$$

were measured over the pressure range from 2 to 10 Torr at 293 K. Previously, Davidson et al.[6] studied the shock tube pyrolysis of NH_3 over the temperature range from 2200 to 2800 K and monitored the temporal dependence of the concentrations of NH and NH_2 using time-resolved high-resolution absorption spectroscopy. The rate constants for both reactions 2a and 3a were determined analyzing a complex reaction mechanism. The reverse of reaction 2a has also been studied in shock tubes by Rohrig and Wagner[7] over the temperature range 1100 to 2000 K. Fontijin et al.[8] used the high-temperature photolysis technique and LIF of NH, and extended the temperature range for the measurement of k_{-2a} to lower temperatures covering the range 833 to 1432 K. The rate constant measurements from both studies were in good agreement. Linder et al.[9] conducted a theoretical study of reaction 2a in both the forward and reverse directions and obtained reasonable agreement with the experimental data. Reaction 3 has not been as widely studied as

* To whom correspondence should be addressed. Fax: (630) 252-9292. E-mail: rgmacdonald@anl.gov.

[†] Current address: National Renewable Energy Laboratory, National Bioenergy Center, 1617 Cole Blvd., Golden, CO 80401.

10.1021/jp809643u CCC: $40.75
Published on Web 02/17/2009

reaction 2a. The only previous direct measurement of k_3 was by Dransfeld et al.[10]at a pressure of 1.1 Torr and 296 K.

In the present work, both NH_2 and NH radicals were generated from the 193 nm laser photolysis of NH_3, and monitored simultaneously following the photolysis laser pulse using time-resolved high-resolution absorption spectroscopy. The NH_2 radical was detected using the $^12_{21} \leftarrow {}^13_{31}$ rotational transition[11] of the $(070)\tilde{A}^2A_1 \leftarrow (000)\tilde{X}^2B_1$ band near 675 nm, and the ground-state $NH(X^3\Sigma^-)$ radical on the $^1R_3(4)$ rotational transition[12] of the $1 \leftarrow 0$ vibrational transition at 3084 nm. The experiments reported on here are directly related to a recent study of the self-reaction of the $NH_2(\tilde{X}^2B_1)$ radical from this laboratory.[13] The rate constants for reactions 2a and 3a were determined by comparing the experimental temporal concentration profiles of NH and NH_2 to those from a detailed chemical model. The mechanism leading to NH formation in the 193 nm photolysis of NH_3 will also be discussed.

2. Experimental Section

The basic experimental apparatus used in this work was similar to that described in previous works.[13−15] Briefly, the transverse flow reaction chamber consisted of a rectangular stainless-steel vessel, containing a Teflon box of dimensions $100 \times 100 \times 5$ cm. The probe laser radiation was multipassed through the rectangular photolysis volume using White-cell optics, increasing the optical path length by a factor of 12 to 1670 cm. The gases flowed continuously through the reaction vessel, and their partial pressures determined from their measured flow rates and total pressure. The NH_3 was admitted to the reaction chamber from a separate glass vacuum line from a large 20 L storage bulb with a coldfinger kept at −40 °C. The gases used were supplied by AGA having the following purities: Ar, 99.995%; CF_4, 99.95%; and NH_3, 99.99%.

The photolysis laser was a Lambda Physik Compex 205 excimer laser operating at a wavelength of 193 nm. Unlike the previous work on NH_2 self-reaction,[13] the attenuation of the photolysis laser by absorption of NH_3 was more than 50%. The partial pressure of NH_3 was varied from 0.01 to 0.035 Torr and was intentionally high in order to generate a detectable concentration of NH.

The visible (Vis) laser was a continuous-wave Environmental Optical Sensors model 2010-ECU external-cavity diode laser, and operated in the red spectral region from 670 to 680 nm. The infrared (IR) laser was a LINOS model 4500 continuous wave OPO laser system. Separate Burleigh Fabry−Perot spectrum analyzers of appropriate finesse and free spectral range continuously monitored the mode quality and the frequency stability of each laser. The frequency of the Vis laser was monitored by a a Burleigh WA150 IR wavemeter with an accuracy of 200 MHz, and the IR laser frequency by a Bristol model 621 wavemeter with an accuracy of 20 MHz. Dichroic mirrors, before and after the White cell optics, spatially overlapped and separated the probe lasers radiation, and directed each to the appropriate detector: a New Focus model 2051 Si detector, for the Vis radiation and a liquid-nitrogen-cooled Cincinnati Electronics InSb detector for the IR radiation. With this arrangement, the temporal dependence of the NH_2 and NH concentrations were monitored simultaneously following the photolysis laser pulse.

Data acquisition and control was provided by a National Instruments PXI system consisting of multiple A/D, D/A and high-speed digitizer modules. The temporal absorption signals were recorded using the two channels of a National Instruments model 5122 14-bit transient recorder operating in the DC mode.

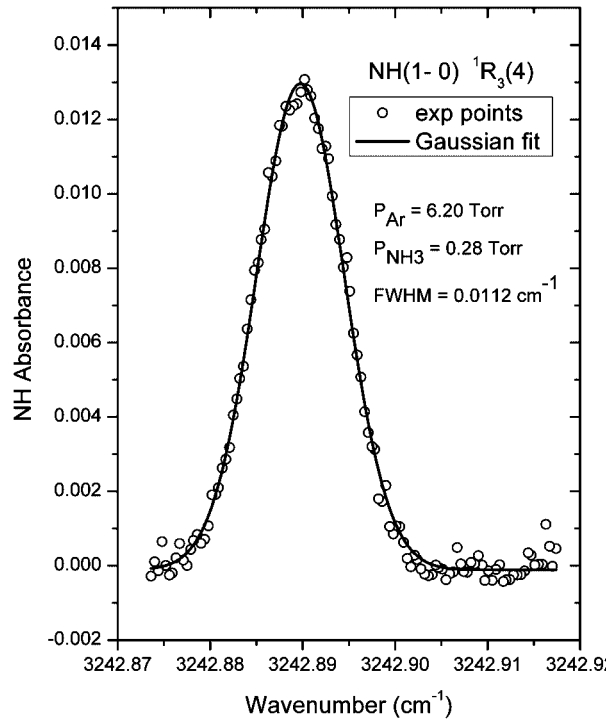

Figure 1. Typical wavelength scan over the $NH(X^3\Sigma^-)(1-0)^1R_3(4)$ absorption line. The open circles (○) are the experimental points, and the line is a fit to the spectrum assuming a Gaussian line profile. The line width (fwhm) is 0.0112 cm^{-1} close to the expected Doppler width of 0.0103 cm^{-1}. The line center transition frequency is 3242.890 $cm.^{-1}$

This allowed the incident Vis laser intensity to be determined directly from the absorption profile using the pretrigger portion of the profile. The initial IR laser intensity was determined from an A/D channel triggered before the excimer laser was fired. The NH absorbance was small, and differential detection of this signal was used to enhance its signal-to-noise ratio. Oscillations on the NH absorption profile due to thermal lensing and refractive index changes induced in the optical elements exposed to the excimer laser radiation were removed by tuning the IR probe laser frequency to a nearby region of zero absorption and recording a background trace. This background profile was subtracted from the signal plus background profile during the data analysis.

Figure 1 shows a frequency scan over the NH $^1R_3(4)$ rotational transition of the ground state $1 \leftarrow 0$ vibrational transition. As is evident from Figure 1, there were no interfering transitions in this spectral region. Note, at this partial pressure of NH_3, the photolysis laser radiation was totally attenuated, and the scan was only used to establish the wavelength at line center. For the rate constant measurements, the NH absorbance was less than 0.5%, and is sufficiently small to prevent accurate determination of the line center by directly tuning the IR laser frequency while photolytically generating the NH radical. The pulse-to-pulse variation in the photolysis laser power and amplitude fluctuations of the probe laser induce too much noise on the box car signal to unequivocally determine the line center form the experimentally generated NH signal. Instead, the good frequency stability of the IR laser, $<3.3 \times 10^{-5}$ cm^{-1} min^{-1}, and the accuracy of the Bristol wavemeter, $\pm 6.7 \times 10^{-4}$ cm^{-1}, were used to preset the IR laser frequency to the line center of the transition and maintain this preset frequency. The wavemeter accuracy corresponds to 6.5% of the full-width at half-maximum (fwhm) Doppler width and falls within the region around line

center that is not strongly frequency dependent. A typical scan over the NH_2 spectral feature was presented previously.[13]

The absorption coefficient at line center for the NH_2 $^1 2_{21} \leftarrow {}^1 3_{31}$ $(070)\tilde{A}^2A_1 \leftarrow (000)\tilde{X}^2B_1$ transition has recently been measured[13] to be $(1.19 \pm 0.23) \times 10^{-17}$ cm^2 molecule^{-1}, under similar experimental conditions as this work. The absorption coefficient at line center for the NH $^1R_3(4)$ rotational transition of the $1 \leftarrow 0$ vibrational transition was calculated from the measurements of the transition moment by Chackerian et al.,[16] and was $(3.25 \pm 0.33) \times 10^{-17}$ cm^2 molecule^{-1}. The uncertainty in both absorption coefficient measurements include estimated systematic and random errors.[17]

3. Results and Discussion

(A) Reaction Mechanism. The complete reaction mechanism describing the $NH_3/NH_2/NH$ system has been presented in detail in a recent work from this laboratory.[13] Reaction 3 is sufficiently rapid that only four reactions account for almost all the reactive flux involving the NH radical. This reaction sequence is given by

$$NH_3 \xrightarrow{193\ nm} NH_3^* \rightarrow NH_2^*/NH_2^\dagger + H$$

$$NH_3^*/NH_2^\dagger \xrightarrow{193\ nm} NH,\ NH^* + H_2/NH,\ NH^* + H$$

$$NH_2 + NH_2 \rightarrow NH(X^3\Sigma^-) + NH_3 \quad \Delta H^0_{0r} = -58\ \text{kJ mol}^{-1} \tag{1a}$$

$$\rightarrow NNH_2 + H_2 \quad \Delta H^0_{0r} = -70\ \text{kJ mol}^{-1} \tag{1b}$$

$$\rightarrow N_2H_2(\text{cis}) + H_2 \quad \Delta H^0_{0r} = -148\ \text{kJ mol}^{-1} \tag{1c}$$

$$\rightarrow N_2H_2(\text{trans}) + H_2 \quad \Delta H^0_{0r} = -170\ \text{kJ mol}^{-1} \tag{1d}$$

$$NH_2 + NH_2 + M \rightarrow N_2H_4 + M \quad \Delta H^0_{0r} = -267\ \text{kJ mol}^{-1} \tag{1e}$$

$$NH_2 + H \rightarrow NH(^3\Sigma^-) + H_2 \quad \Delta H^0_{0r} = -46\ \text{kJ mol}^{-1} \tag{2a}$$

$$NH_2 + H + M \rightarrow NH_3 + M \quad \Delta H^0_{0r} = -444.1\ \text{kJ mol}^{-1} \tag{2b}$$

$$NH_2 + NH \rightarrow NH_3 + N(^4S_u) \quad \Delta H^0_{0r} = -117\ \text{kJ mol}^{-1} \tag{3a}$$

$$\rightarrow N_2H_2 + H(^2S) \quad \Delta H^0_{0r} = -124\ \text{kJ mol}^{-1} \tag{3b}$$

$$NH_2 + NH + M \rightarrow N_2H_3 + M \quad \Delta H^0_{0r} = -314\ \text{kJ mol}^{-1} \tag{3c}$$

$$X \rightarrow \text{diffusion} \tag{13}$$

where the * indicates electronically excited states, the † highly excited internal states, and X any species in the mechanism. The complete reaction mechanism is summarized[18−25] in Table 1. The enthalpies of all the species used in the data analysis have been given.[13] Unlike the previous study of the NH_3/NH_2 system from this laboratory, diffusion does not contribute significantly to the loss of NH because the reaction time is short. Nevertheless, the first-order diffusion rate constants were included in the data analysis, and calculated by the procedure outlined previously[26] using the diffusion rate constants previously determined[13] for NH_3. The reaction sequence producing the NH radical, indicated by the second photolysis step in the above reaction sequence, is unknown but will be further discussed in section C. However, the appearance of NH is sufficiently rapid compared to its removal that its production can be accounted for by extrapolating the NH concentration profile to time zero. Reaction 1a contributes to the production of NH; however, k_{1a} used in the data analysis is not well established. As discussed previously,[13] the value used was taken as the upper bound established by Dransfeld et al.[10] This estimate is in agreement with a theoretical calculation.[20] In a recent work,[13] we have shown that at the pressures used in the present experiment the rate constant for reaction 1 can be represented by a linear function of carrier gas pressure. The intercept is the

TABLE 1: Chemical Model Influencing the NH_2 + NH Reaction at 293 K

no.	reactants		products	k (cm^3 molecule^{-1} s^{-1})[a,b]	ref
1a	$NH_2 + NH_2$	→	$NH(X^3\Sigma^-) + NH_3$	3.0×10^{-15}	10
1b		→	$NNH_2 + H_2$	(3.4×10^{-13})[c]	13
1c		→	$N_2H_2(\text{cis}) + H_2$		
1d		→	$N_2H_2(\text{trans}) + H_2$		
1e	$NH_2 + NH_2 + CF_4$	→	$N_2H_4 + CF_4$	8.0×10^{-29}	13
1e	$NH_2 + NH_2 + Ar$	→	$N_2H_4 + Ar$	3.9×10^{-29}	13
2a	$NH_2 + H$	→	$NH + H_2$	7.7×10^{-15}	this work
2b	$NH_2 + H + M$	→	$NH_3 + M$	6.0×10^{-30} [M][d]	18
3	$NH_2 + NH$	→	$N_2H_2 + H$	9.6×10^{-11}	this work
4a	$NH + NH$	→	$N_2 + 2H$	3.4×10^{-12}	19
4b		→	$NH_2 + N$	4.0×10^{-13}	20
5	$NH + H$	→	$H_2 + N$	3.2×10^{-12}	21
6	$H + H + M$	→	$H_2 + M$	1.0×10^{-33} [M][d]	22
7	$H + N_2H_2$	→	$H + H_2 + N_2$	3.0×10^{-13}	9
8	$H + N_2H_4$	→	$H_2 + N_2H_3$	1.5×10^{-13}	23
9	$NH_2 + N_2H_4$	→	$NH_3 + N_2H_3$	5.3×10^{-13}	24
10a	$H + N_2H_3$	→	$H_2 + N_2H_2$	1.7×10^{-11}	25
10b		→	$NH_2 + NH_2$	2.6×10^{-12}	24
11	$NH + N_2H_3$	→	$N_2H_2 + NH_2$	3.3×10^{-11}	25
12	$NH_2 + N_2H_3$	→	$N_2H_2 + NH_3$	2.8×10^{-12}	25
13	X	→	X(diffusion)[e]		13

[a] Second-order rate constants units, cm^3 molecule^{-1} s^{-1}. [b] Third-order rate constants units, cm^6 molecule^{-2} s^{-1}. [c] The sum of the second-order processes, $k_{1,0} = k_{1a} + k_{1b} + k_{1c} + k_{1d}$. [d] Third body efficiency of CF_4 and Ar assumed equal to NH_3. [e] X represents each species in the mechanism.

sum of the rate constants for the disproportionation channels, $k_{1,0} = k_{1a} + \Sigma_i^d{}_{=b} k_{1i}$, and the slope represents the third-body dependent recombination reaction rate constant, $k_{1e,0}^{M}$. These rate constants and associated uncertainties were measured to be $k_{1,0} = (3.4 \pm 6) \times 10^{-13}$ cm^3 molecule^{-1} s^{-1}, and $k_{1e,0}^{CF_4} = (8.0 \pm 0.5) \times 10^{-29}$, and $k_{1e,0}^{Ar} = (3.9 \pm 0.4) \times 10^{-29}$ cm^6 molecule^{-2} s^{-1}. Reaction 2b is not well established but has been measured[18] to be 6.0×10^{-30} cm^6 molecule^{-2} s^{-1} for NH_3 as third body. The signal-to-noise of the NH profiles was sufficient to obtain an experimental determination of k_{2a}.

The products of reaction 3 have not been identified experimentally or investigated theoretically, but have been discussed by Dean and Bozzelli.[4] These workers estimated the activation energy for reaction 3a using the Evans Polanyi relationship to be 10.2 kJ mol^{-1}. This large activation barrier would preclude reaction 3a from being important at 293 K, and it was not considered in the data analysis. These workers also suggest reaction 3b would likely be the dominant product channel. On the basis of isoelectonic sequences, Miller et al.[27] also suggested that reaction 3b was the dominant product channel. In the data analysis, reaction 3b was taken to be the only product channel. As will be shown in the next section, k_3 was found to be pressure independent, and channel 3c is unlikely to be the dominant reaction channel. In any case, the initial concentration of the NH radical is so small and k_3 rapid enough that the products of reaction 3 cannot influence the kinetics of the NH radical.

(B) Determination of k_{2a} and k_3. As described in a recent work, rate constants were determined by minimizing the sum of the squares of the residuals, χ^2, between the observed NH temporal concentration profile to one generated from a computer simulation using the rate constants summarized in Table 1. An integrated reaction contribution factor, $IRCF_{Y+Z}^{X}$, analysis[28] was also included in the data reduction to determine the extent a particular reaction, Y + Z, contributed to the production or removal of a particular species, X, in the reaction mechanism. The $IRCF_Y{}^X{}_{+Z}$s were expressed as a fraction of the total concentration of species X produced or removed in the system, and represent the fraction of the total flux of species X that proceeded through reaction Y + Z during a given time interval.

Figures 2 and 3 show typical NH_2 and NH temporal concentration profiles obtained under low and high initial NH concentration conditions, respectively. In each case, the corresponding NH_2 and NH concentration profiles were obtained on the same photolysis laser pulse. In both figures, the experimental data points, the solid circles (•), are shown for the first 50 μs for every data point, and the open circles (○) are shown every fifth data point. The solid lines are the model generated concentration profiles NH_2 and NH resulting in the variation of k_1 and k_{2a} and k_3, respectively. As is evident from the Figures, the initial NH concentration was much smaller than the initial NH_2 concentration. Although the NH_2 concentration is in large excess over the NH concentration, the NH concentration profile decay cannot be described by a single exponential curve so that pseudofirst order conditions are not appropriate for this system. Both reactions 1a and 2a contribute significant NH product flux and must be accounted for in the data analysis.

As can be seen from Figures 2b and 3b, the NH($X^3\Sigma^-$) radical was not formed directly by photolysis of NH_3, but was produced with a pressure dependent rate over several tens of microseconds. The shape of the temporal concentration profile of NH($X^3\Sigma^-$) suggests that it was formed from the quenching of a precursor created in the 193 nm photolysis of NH_3. The induction period for NH formation was accounted for by extrapolating the concentration profiles of NH to time zero and

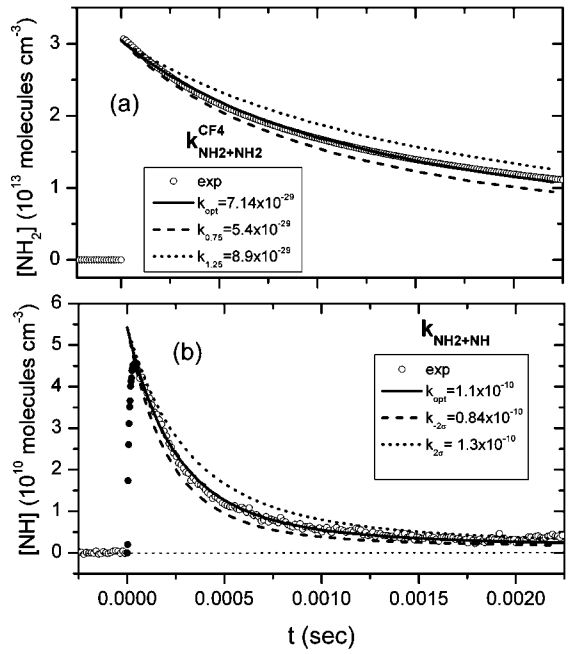

Figure 2. Typical temporal concentration profiles for (a) NH_2 and (b) NH. Both concentration profiles were recorded simultaneously following the 193 nm photolysis pulse. The conditions of the experiment were $P_{NH_3} = 0.013$ and $P_{CF_4} = 4.663$ Torr at a nominal ArF laser fluence of 25 mJ cm^{-2} and 294 K. (a) NH_2 experimental data points are shown by the open circles (○) every fifth point. The solid line is the model fit to the NH_2 profile to determine k_{1e} to be 7.1×10^{-29} cm^6 molecule^{-2} s^{-1}, and the dashed lines are variation in the NH_2 concentration profile for a ± 25% variation in k_{1e}. (b) Experimental data points for NH shown by the closed circles (●) every data point for the first 50 μs and every fifth data point by the open circles (○). The solid line is the model simulation of the NH profile with $k_{2a} = 1.0 \times 10^{-14}$ cm^3 molecule^{-1} s^{-1} and $k_3 = (1.05 \pm 0.25) \times 10^{-10}$ cm^3 molecule^{-1}s^{-1}, where the uncertainty is $\pm 2\sigma$ in the goodness of fit.

proceeding with the model simulations using this initial NH concentration. However, the comparison between model simulations and experimental profiles was delayed for 100 μs. The initial concentration of NH was determined by fitting the NH profiles to a series of three exponential terms of the form: $(Ae^{-k_a t} + Be^{-k_b t}) - Ce^{-k_c t}$. The two terms with positive pre-exponential factors described the decay of the NH profile and the term with the negative pre-exponential factor described the rise in the NH concentration profile. The concentration of NH at time zero was approximated by the sum, $A + B$. Simply extrapolating the NH concentration profiles back to time zero would also have been sufficiently accurate, but the production term, k_c, was used in an unrelated calculation to provide some insight into the mechanism of NH radical production. This calculation will be discussed in the following section. The above analysis assumes that the NH ro-vibrational states have equilibrated to the temperature of the bath gas over the time scale of the production of NH. With CF_4 as a bath gas, vibrational equilibrium was established in a few microseconds for both NH_2 and NH_3 following the photolysis pulse and with a small addition of CF_4 (less than 0.4 Torr) to an Ar bath gas to less than 10 μs.[13] Vibrational relaxation of NH by CF_4 is also likely rapid.

To create a detectable concentration of NH, it was necessary to use much larger concentrations of NH_3 than used in the previous experiments conducted in this laboratory.[13] Thus, the axial distribution of the radicals had a much larger gradient than in previous work, and it is possible this could influence[14] the measurement of k_3. However, the measurements of k_1 in the present work were found to be within 10% of the previously

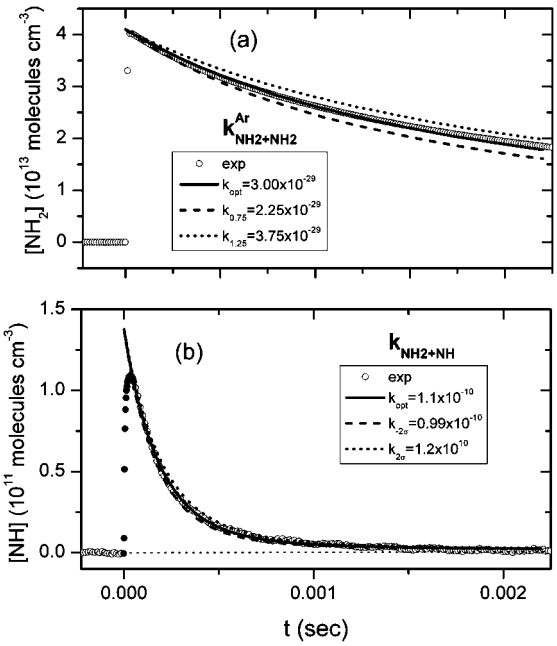

Figure 3. Similar to Figure 2 except Ar is the major carrier gas, giving an increase in the initial concentration of NH. The conditions of the experiment were $P_{NH_3} = 0.016$, $P_{CF_4} = 0.296$, and $P_{Ar} = 4.600$ Torr at a nominal ArF laser fluence of 26 mJ cm^{-2} and 293 K. (a) Same as Figure 2a except $k_{1e}^{CF_4} + k_{1e}^{Ar} = 3.0 \times 10^{-29}$ cm^6 molecule^{-2} s^{-1}. (b) Same as Figure 2b except $k_3 = (1.10 \pm 0.10) \times 10^{-10}$ cm^3 molecule^{-1} s^{-1}.

reported measurements from this laboratory,[13] so such effects were small. The determination of k_3 was not sensitive to the exact value of $k_{1e,0}^M$ used in the data analysis. In Figures 2a and 3a, the solid lines show the concentration profiles for NH_2 predicted by the model simulations using the optimum fit values for $k_{1e,0}^M$, and the dashed lines show the NH_2 concentration profiles predicted for a variation of ±25% in the values of $k_{1e,0}^M$. If these larger or smaller values for $k_{1e,0}^M$ were used in the reaction mechanism to determine the new values for k_3, the NH profiles would be indistinguishable from the solid lines in Figures 2b and 3b, and the change in optimum value of k_3 would be about ±2%.

As noted above, reactions 1a and 2a were sources for the production of NH, and contributed to the observed kinetics for NH. The production flux of NH from these two sources was of the order of 20% of the total removal flux of NH so that even though k_{1a} and k_{2a} were small (Table 1), the NH_2 and H atom concentrations were hundreds of times larger than the NH radical concentration, making these two reactions important. Their impact on the production of NH is clearly seen as the slow approach of the NH concentration profile to the baselines in Figures 2b and 3b. Neither k_{1a} nor k_{2a} have been measured experimentally at 293 K, but an experimental upper limit of k_{1a} equal to 3.0×10^{-15} cm^3 molecule^{-1} s^{-1} has been established.[10] This value was kept constant in the data analysis and k_{2a} varied. The procedure adopted to optimize k_3 and k_{2a} was similar to that described previously.[26] The initial value of k_{2a} was set to zero, and the optimum value of k_3 determined. The value of k_{2a} was incremented by 5×10^{-15} and the new optimized value of k_3 determined for this value of k_{2a}. These steps were repeated until a minimum in $\chi^2(k_{2a}, k_3)$ was identified. In Figure 2a, the solid curve is the model generated concentration profile for these optimum values of k_{2a} and k_3 equal to 1.0×10^{-14} and $(1.05 \pm 0.2) \times 10^{-10}$ cm^3 molecule^{-1} s,$^{-1}$ respectively. The uncertainty in k_3 is the 95% confidence limit in the goodness-of-fit. The dashed curves are the NH profiles calculated using these confidence limits for k_3. The variation of k_3 with a change of k_{2a} from 0 to 2.0×10^{-14} cm^3 molecule^{-1} s^{-1} would result in change in k_3 of about ± 10%, and be well within the limits shown in the figure. For this experiment, the $IRCF_{NH_2+H}^{NH}$ was three times larger than the $IRCF_{NH_2+NH_2}^{NH}$, as expected from the ratio of the two rate constants and the approximately equal NH_2 and H atom concentrations. Figure 3b is similar to Figure 2b except for a higher initial NH concentration, and hence, has a higher signal-to-noise ratio. The parameter set that produced the best fit to the data was k_{2a} equal to 1.0×10^{-14} and k_3 equal to $(1.06 \pm 0.08) \times 10^{-10}$ cm^3 molecule^{-1} s^{-1}. The dashed curves are again the model generated NH concentration profiles for the limits of k_3 at the ±2σ range of uncertainty.

The experimental conditions and results are summarized in Table 2 for the experiments in CF_4 as bath gas and in Table 3 for mixtures of Ar with a small amount of added CF_4 to facilitate vibrational relaxation, as discussed below.

With k_{1a} set at 3.0×10^{-15} cm^3 molecule^{-1} s^{-1}, k_{2a} was determined to be $(7.7 \pm 14) \times 10^{-15}$ cm^3 molecule^{-1} s^{-1}, where the uncertainty is ±2σ in the scatter of the data. The measurements of k_{2a} equal to 5.0×10^{-14} cm^3 molecule^{-1} s^{-1} were ignored in determining the value of k_{2a}. The value of k_3 was found to be $(9.6 \pm 2.0) \times 10^{-11}$ cm^3 molecule^{-1} s^{-1}, where the uncertainty is ±2σ in the scatter of the data. Figure 4a shows that within the scatter of the data k_3 was independent of the initial NH concentration and the nature of the carrier gas, whether it was in CF_4, (•) or dilute CF_4/Ar mixtures (□). The photolytic yield of NH was slightly higher in dilute CF_4/Ar mixtures, and as can be seen from Figure 4a, the experiments involving the highest initial NH concentration were conducted using dilute CF_4/Ar mixtures. The CF_4 was added to facilitate the rapid vibrational relaxation of NH_2. The vibrational relaxation rate constant[29] of $NH_2(0,v_2,0)$ by CF_4 as collision partner is very large, 3.2×10^{-11} cm^3 molecule^{-1} s^{-1}. Also, work from this laboratory[13] showed the addition of a few tenths of a Torr of CF_4 to Ar dramatically reduced the equilibration time for both NH_2 and NH_3 from hundreds of microseconds to a few microseconds. The independence of the measurements of k_3 on the initial NH concentration indicated that the NH ro-vibrational states had also rapidly equilibrated to the carrier gas temperature either in collisions with CF_4 or because of the pressures of the experiments. Figure 4b shows that the measurements of k_3 were independent of the total pressure and composition of the carrier gas, within the scatter of the data. Although the pressure range is not large, Figure 4b suggests that reaction 3 is dominated by the disproportionation channel because k_3 was independent of the nature of both the carrier gas and pressure. Under similar conditions, reaction 1 is dominated by the recombination channel.

(C) Production and Yield of NH($X^3\Sigma^-$) in the 193 nm Photolysis of NH_3. The exact mechanism of the generation of NH from the 193 nm photolysis of NH_3 is complex, and is not completely understood.[30,31] For the present work, it is clear from Figures 2b and 3b that no NH($X^3\Sigma^-$) was observed immediately after the photolysis pulse. The production rate of NH($X^3\Sigma^-$) linearly increased with total pressure, and yielded a rate constant of $(5.9 \pm 1.1) \times 10^{-13}$ cm^3 molecule^{-1} s^{-1} in CF_4 and $(8.5 \pm 1.4) \times 10^{-13}$ cm^3 molecule^{-1} s^{-1} in dilute CF_4/Ar mixtures. The initial yield of NH from the 193 nm photolysis of NH_3, defined as the initial concentration of NH($X^3\Sigma^-$) divided by the initial concentration of NH_2, was (0.0016 ± 0.00017) in CF_4 and (0.0032 ± 0.0005) in dilute CF_4/Ar mixtures.

TABLE 2: Summary of the Experimental Conditions and Measurements of k_{2a} and k_3 in CF_4 at 293 K

partial pressure (Torr)		$[NH]_0 \times 10^{-10}$	$[NH_2]_0 \times 10^{-13}$	$k_{2a} \times 10^{14}$	$k_3 \times 10^{11}$
P_{CF_4}	P_{NH_3}	(molecules cm^{-3})	(molecules cm^{-3})	(cm^3 $molecule^{-1}$ s^{-1})[a,b]	(cm^3 $molecule^{-1}$ s^{-1})
2.85	0.00745	3.86	1.79	5.0[a]	11.2 (± 3.3)[b]
2.85	0.00745	4.38	1.94	5.0	11.0 (± 3.3)
2.85	0.00745	3.92	1.88	5.0	14.0 (± 4.4)
2.88	0.0173	8.61	3.63	2.0	8.6 (± 1.7)
2.99	0.00843	3.78	2.31	0.1	9.8 (± 1.3)
2.99	0.00843	4.55	2.36	2.0	8.8 (± 2.1)
3.32	0.0087	3.98	2.34	0.1	9.8 (± 1.0)
3.32	0.0087	4.10	2.36	0.5	9.0 (± 0.42)
3.66	0.0219	9.56	4.63	1.0	8.6 (± 0.84)
3.66	0.0219	8.81	4.67	0.1	7.73 (± 2.1)
4.17	0.0109	4.85	2.59	2.0	10.0 (± 1.3)
4.17	0.0109	5.03	2.66	1.0	9.6 (± 0.63)
4.18	0.0118	5.37	2.91	1.0	10.0 (± 2.1)
4.18	0.0118	6.63	2.84	2.0	10.0 (± 2.5)
4.54	0.0273	10.4	5.00	0.1	8.9 (± 0.84)
4.54	0.0273	11.0	5.09	0.5	8.52 (± 0.84)
4.66	0.0130	5.43	3.05	0.5	10.5 (± 2.5)
4.66	0.0130	5.50	3.12	0.5	11.6 (± 1.7)
5.07	0.0141	5.76	3.27	1.0	8.7 (± 0.84)
5.36	0.0322	11.5	5.74	0.5	8.5 (± 1.3)
5.55	0.0145	4.85	3.11	0.1	11.9 (± 1.7)
5.55	0.0145	5.23	3.12	0.1	9.2 (± 2.5)
5.90	0.0165	6.17	3.40	1.0	9.2 (± 1.3)
5.90	0.0165	6.42	3.60	1.0	8.7 (± 1.0)
5.94	0.0356	12.6	6.05	0.1	8.7 (± 0.84)
6.31	0.0176	6.04	3.66	0.5	8.7 (± 1.0)
6.31	0.0176	6.35	3.63	0.5	9.4 (± 2.5)
6.37	0.0388	12.3	6.19	0.1	8.1 (± 2.5)
6.38	0.388	12.4	6.19	1.0	8.3 (±1.3)
6.49	0.0169	6.43	4.14	0.1	8.3 (± 2.1)
6.49	0.0169	6.50	4.18	0.5	10.1 (± 2.5)
6.69	0.0377	11.1	5.94	2.0	9.1 (± 2.5)
7.13	0.0200	7.31	3.72	2.0	8.8 (± 2.5)
7.21	0.0188	6.28	3.73	0.1	11.1 (± 0.84)
7.21	0.0188	6.28	3.73	0.5	11.2 (± 0.53)
7.58	0.0356	10.3	6.02	0.5	9.1 (± 0.84)
7.68	0.0200	6.01	3.68	0.5	8.8 (± 1.9)
7.68	0.0200	7.45	3.73	1.0	9.5 (± 0.81)
7.80	0.0220	6.54	3.84	1.0	8.6 (± 1.7)
8.13	0.0212	7.34	3.61	0.5	10.3 (± 3.3)
8.13	0.0212	6.36	3.92	0.5	8.4 (± 0.48)
8.75	0.0364	11.1	5.82	0.1	8.8 (± 0.95)
8.75	0.0364	11.2	5.82	0.1	8.7 (± 0.75)
8.75	0.0364	10.5	6.13	1.0	8.4 (± 1.3)
8.75	0.0364	11.0	6.13	1.0	8.2 (± 1.3)
8.78	0.0229	5.42	3.33	0.1	10.7 (±0.90)
8.78	0.0229	5.83	3.31	2.0	10.4 (± 1.7)
8.78	0.0229	6.47	3.84	0.1	9.5 (± 2.1)
8.78	0.0229	6.16	4.07	0.1	9.9 (± 1.3)
9.65	0.0251	6.45	4.08	0.5	6.7 (± 2.5)
9.65	0.0251	6.50	4.12	0.5	10.3 (± 0.30)

[a] k_{2a} incremented in steps of 5.0×10^{-15} cm^3 $molecule^{-1}$ s^{-1}. [b] Uncertainty is $\pm 2\sigma$ in the goodness of fit to the NH concentration profiles.

Kaes and Stuhl[30] have discussed the formation of $NH(X^3\Sigma^-)$ in the 193 nm photolysis of NH_3 in dilute NH_3/Ar mixtures and ArF fluences similar or higher to those used in this work. They noted that the temporal appearance of the $NH(X^3\Sigma^-)$ profile suggested that it was formed from the collisional quenching of some precursor formed in the photolysis of NH_3. These workers found no consistent model to describe the temporal behavior of NH. At Ar pressures of 2 Torr, the appearance rate constant was similar to that observed in the present work, but unlike the present work it decreased with increasing Ar pressure. They also observed that some fraction of $NH(X^3\Sigma^-)$ was formed directly following the photolysis laser pulse. This latter process has been identified by Kenner et al.[32] as a sequential two photon process in which a second 193 nm photon was absorbed by highly excited internal states of $NH_2(\tilde{X}^2B_1)$, creating $NH(A^3\Pi)$. Subsequent fast radiative decay (radiative lifetime of 0.42 μs) and near gas kinetic quenching[31] of $NH(A^3\Pi)$ produced $NH(X^3\Sigma^-)$. In the present experiment, this pathway may have been suppressed because the addition of a small amount of CF_4 has been shown[13] to rapidly remove highly excited states of $NH_2(\tilde{X}^2B_1)$.

The simplest possible precursor to $NH(X^3\Sigma^-)$ formation is the initial formation of a metastable excited electronic state of NH. Metastable states of NH have been observed following the 193 nm photolysis of NH_3 in one[33] ($NH(a^1\Delta)$) or two photon[34] ($NH(b^1\Sigma^+)$) processes. However, there is not a great deal of information available about the collisional quenching[35,36] of $NH(a^1\Delta)$ or $NH(b^1\Sigma^+)$. Generally, $NH(b^1\Sigma^+)$ is quenched at

TABLE 3: Summary of the Experimental Conditions and Measurements of k_{2a} and k_3 in Ar at 293 K

partial pressure (Torr)			$[NH]_0$ ($\times 10^{-10}$)	$[NH_2]_0$ ($\times 10^{-13}$)	k_{2a} ($\times 10^{14}$)	k_3 ($\times 10^{-11}$)
P_{Ar}	P_{CF_4}	P_{NH_3}	(molecules cm^{-3})	(molecules cm^{-3})	(cm^3 molecle^{-1} s^{-1})	(cm^3 molecle^{-1} s^{-1})
2.08	0.134	0.00726	9.05	1.83	1.0[a]	10.6 (± 3.3)[b]
2.87	0.184	0.0100	11.4	2.97	0.1	10.7 (± 0.42)
3.26	0.10	0.0114	13.1	3.13	5.0	9.6 (± 2.9)
3.95	0.254	0.0138	13.8	3.31	5.0	12.0 (± 1.7)
4.60	0.296	0.0161	13.4	4.09	2.5	10.9 (± 1.7)
4.60	0.296	0.0161	13.8	4.10	1.0	10.6 (± 0.84)
5.31	0.341	0.0185	14.6	4.25	1.0	10.5 (± 2.1)
6.30	0.404	0.0220	15.9	4.95	0.5	9.9 (± 1.3)
6.578	0.422	0.0230	17.4	4.84	5.0	10.2 (± 2.5)
6.578	0.422	0.0230	15.2	4.84	0.5	10.5 (± 2.1)
7.56	0.487	0.0265	16.1	5.43	2.0	9.1 (± 0.84)
7.58	0.487	0.0265	16.6	5.42	0.1	9.4 (± 1.7)
8.00	0.514	0.0279	16.5	5.55	5.0	10.7 (± 3.3)
9.18	0.590	0.0321	16.4	5.47	2.0	10.0 (± 2.5)

[a] k_{2a} incremented in steps of 5.0×10^{-15} cm^3 molecule^{-1} s^{-1}. [b] Uncertainty is $\pm 2\sigma$ in the goodness of fit to the NH concentration profiles.

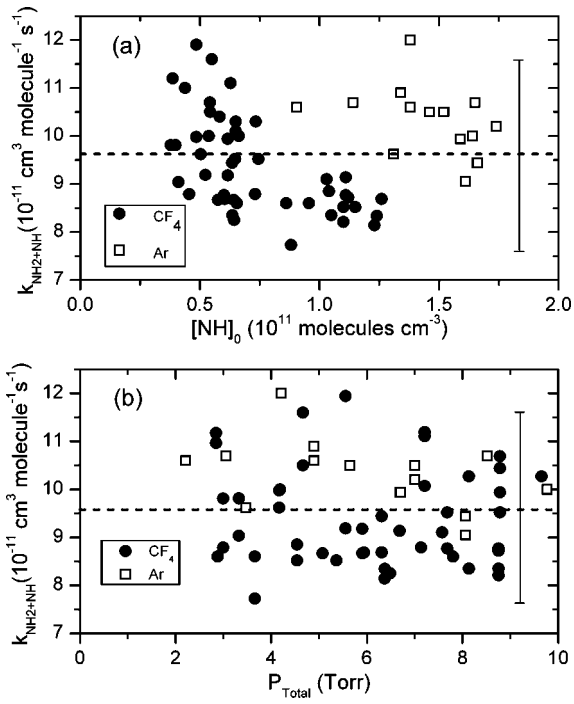

Figure 4. (a) Rate constant measurements for k_3 as a function of the initial NH concentration. The measurements with CF_4 as carrier gas are shown by the solid circles (●) and with dilute CF_4/Ar by the open squares (□). The dashed line is the average value of the k_3, and the vertical line is the $\pm 2\sigma$ level of uncertainty in the scatter of the data. (b) Same as (a) except k_3 is shown as a function of total pressure. The measurements of k_3 in CF_4 are indicated by the solid circles (●) and in dilute CF_4/Ar mixtures by the open squares (□).

slower rates than NH($a^1\Delta$) by the same collision partners. Piper et al.[37] measured the quenching rate constant of NH($a^1\Delta$) by Ar to be 1.2×10^{-14} cm^3 molecule^{-1} s^{-1}, and Rohrer and Stuhl[38] placed an upper limit on this rate constant of 1.0×10^{-15} cm^3 molecule^{-1} s^{-1}. There is no data available for the quenching of NH($a^1\Delta$) by CF_4. Further complications come from the rapid reaction between NH($a^1\Delta$) and NH_3. The rate constant for the reaction, NH($a^1\Delta$) + $NH_3 \rightarrow 2NH_2$ has been measured to be 1.5×10^{-10} cm^3 molecule^{-1} s^{-1} at 293 K, and the product channel identified.[39] In spite of the inconsistency in the literature Ar quenching rate constant of NH($a^1\Delta$) and the measured rate of appearance of NH($X^3\Sigma^-$) in the current experiment, it is useful to model the system to estimate the initial yield of the precursor of NH($X^3\Sigma^-$) in the photolysis of NH_3. The different initial yields of NH($X^3\Sigma^-$) in CF_4 and Ar suggests a competition between NH($X^3\Sigma^-$) formation and another pathway in the collisional quenching of the precursor. The alternate pathway was taken as the rapid reaction of the precursor with NH_3, similar to the situation if the precursor was NH($a^1\Delta$). Thus, the yield of NH($X^3\Sigma^-$) in each experimental record was corrected for the loss of the precursor by a rapid reaction with NH_3. This analysis gives the initial yield of NH($a^1\Delta$) to be (0.0081 ± 0.0025) in CF_4 and (0.0096 ± 0.0027) in dilute CF_4/Ar mixtures. The average of these measurements gives the initial yield of NH($a^1\Delta$) to be (0.0088 ± 0.0026). The agreement within the scatter of the measurements suggests that the model may have some validity. This estimate is in agreement with an upper limit to the yield of NH($a^1\Delta$) measured to be 0.008 by Kenner et al.,[33] and at least indicates that the process leading to NH($X^3\Sigma^-$) formation does not have a large yield. Vibrationally excited NH($X^3\Sigma^-$) was detected by Kaes and Stuhl,[30] and could influence the interpretation of the appearance rate of NH($X^3\Sigma^-$)($v = 0$) observed in the present experiments. However, the determination of k_3 was independent of both pressure and initial NH concentration, indicating vibrational relaxation was fast with CF_4 in the gas mixture.

As noted, the model just described above assumes the precursor to NH($X^3\Sigma^-$) was NH($a^1\Delta$), but it is likely some other species. However, the model does explain the variation of the yield of NH($X^3\Sigma^-$) with collision partner. The precursor must be formed rapidly; it must react rapidly with NH_3 so that there is a competition between production of NH($X^3\Sigma^-$) and another process; it must be efficiently quenched in collisions with Ar and CF_4. It is also possible that there are other sources or processes responsible for the production of NH($X^3\Sigma^-$) rather than the quenching of electronically excited states of NH.[31] In any case, the yield of the NH($X^3\Sigma^-$) precursor was small, and the production rate constant of NH($X^3\Sigma^-$) sufficiently large that the exact mechanism of NH production did not influence the observed kinetics and determination of the rate constants.

(D) Estimated Uncertainty in k_3. The two main systematic sources of error in the measurement of k_3 are the uncertainty in the rate constants used to model the chemistry of the system and the uncertainty in determining the concentrations of the NH_2 and NH radicals. It has already been discussed in section III B that the determination of k_3 was very weakly dependent on the value used for k_1, a variation of ± 25% in k_1 resulted in a change of k_3 of a few percent so that uncertainties in the rate constants in Table 1 had a small effect on the determination of k_3.

However, k_{2a} and k_3 were both treated as variables in the data analysis; the value of k_{2a} also affects the value of k_3. For the complete data set, a variation of k_{2a} ranging form 0 to 2.0×10^{-14} cm^3 molecule^{-1} s^{-1} resulted in a variation in k_3 of $\pm$ 10%. This variation in k_{2a} is slightly larger than the scatter in the determination of k_{2a} at the 2σ confidence limit, but represents a good estimate of the influence the uncertainty in k_{2a} has on the determination of k_3. Combining the uncertainty in the scatter of k_3 ($\pm$21%) with the influence of k_{2a} ($\pm$10%) results in the total uncertainty in k_3 from these sources of $\pm$23%.

As noted above, the NH concentration profile is dominated by reaction 3, and hence, the determination of k_3 with an uncertainty including systematic and random errors of $\pm$23%. However, the uncertainty in the scatter of k_{2a}, $\pm$180%, dominates the total uncertainty in k_{2a} and can be taken as the total uncertainty including systematic and random error.

The uncertainty in the NH_2 absorption coefficient including systematic and random errors has been discussed[13] and was $\pm$19% at the 2σ level of confidence. The uncertainty in the NH absorption coefficient was estimated to be $\pm$10% at the 2σ confidence limit including systematic and random errors. This estimate was based on the scatter of the experimental measurements[16] of the transition dipole moment and its close agreement with a high-level theoretical calculation.[17] The combined uncertainty from the determination of the radicals concentrations was $\pm$22% at the 2σ level of confidence.

All other sources of uncertainty are much smaller than those just discussed; thus, the total uncertainty in the determination of k_3 arising from the reaction model and absorption coefficient determination was $\pm$23% and $\pm$22%, respectively. These sources of uncertainty are uncorrelated and can be combined to give a total uncertainty in k_3 of $\pm$32%, including systematic and random error at the 2σ level of confidence. Similarly, the estimated uncertainty in k_{2a} was $\pm$180%.

(E) Comparison the Previous Work. There are no previous low temperature measurements of k_{2a}. Davidson et al.[6] provide an Arrhenius expression for k_{2a} derived from their high temperature measurements. Extrapolating this expression to 293 K gives an estimate of k_{2a} equal to 1.2×10^{-13} cm^3 molecule^{-1} s^{-1}. This value is fifteen times larger than the value measured in the present work. Of course, the extrapolation from 2200 to 300 K is long and cannot be expected to provide an accurate prediction of the rate constant near room temperature. The theoretical calculations of Linder et al.[9] provide a better estimate of k_{2a}. These workers used high-level ab initio electronic structure theory to characterize the $NH_2 + H$ PES and canonical variational transition state theory to calculate rate constants in both the forward and reverse directions. The calculated rate constants also included corrections for tunneling and anharmonicity effects. These workers calculated both forward and reverse rate constants that were in reasonable agreement with the experimental data. These calculations covered the temperature range 500 to 3000 K. An extrapolation of the temperature dependence to 293 K gives k_{2a} equal to 4.1×10^{-14} cm^3 molecule^{-1} s^{-1}. This is within a factor of 5 of the measurements of the present work and should be considered reasonable agreement, considering the large uncertainty associated with the experimental measurements reported here.

As noted in the introduction, there is only one previous measurement of k_3 at 296 K by Dransfeld et al.[10] These workers used a discharge flow system of NH_3/F_2/He mixtures to generate NH_2 and NH from the reactions $F + NH_3$ and $F + NH_2$ in varying mixtures of excess NH_3 over the initial F atom concentration. Thus, the measurements were made under pseudo-first-order conditions with the NH_2 concentration in excess. Laser magnetic resonance spectroscopy was used to determine the absolute concentration of the NH and NH_2 radicals and follow the temporal decay of the NH radical concentration. The rate constant for reaction 3 was measured to be $(1.3 \pm 0.5) \times 10^{-10}$ cm^3 molecule^{-1} s,$^{-1}$ where the uncertainty is $\pm 2\sigma$ in the scatter of the measurements. These measurements and the measurements of the present work are within their associated uncertainties and in good agreement with each other.

As noted in the introduction, reaction 3 is typical of the complexity of radical−radical reactions. The reagents correlate to quartet and doublet spin manifolds leading to different product channels in each manifold. In the doublet manifold, the reaction occurs under the influence of the deep N_2H_3 potential well. The N_2H_3 complex has a lower energetic asymptote than the reactants, and can dissociate to $N_2H_2 + H$ products. Thus, reactions 3b and 3c represent the classic competition between adduct formation, stabilization, and fragmentation to products. This behavior is typical for radical−radical reactions especially involving nitrogen-containing species as recently highlighted in detail by Fernández-Ramos et al.[40] for the $NH_2 + NO$ reaction.

4. Conclusion

The 193 nm photolysis of NH_3 was used to generate both the NH_2 and NH radical. The temporal concentration profiles of both species were monitored simultaneously using time-resolved high-resolution absorption spectroscopy. The production of the NH($X^3\Sigma^-$) radical was interpreted as the quenching of a precursor created in the 193 nm photolysis of NH_3, perhaps NH($a^1\Delta$), by the carrier gas in competition with rapid removal by NH_3. This model predicted that the yield of the precursor to be 0.0088 ± 0.0026. Separately, the yield of NH($X^3\Sigma^-$) at ArF laser fluences of about 30 mJ cm^{-2} was measured to be 0.0016 and 0.0032 in CF_4 and dilute CF_4/Ar mixtures, respectively. The system was analyzed used a detailed chemical model, summarized in Table 1 for the NH chemistry. The rate constant for reaction 2a was found to be $(7.7 \pm 14) \times 10^{-15}$ cm^3 molecule^{-1} s^{-1}, and for reaction 3 was measured to be $(9.6 \pm 3.2) \times 10^{-11}$ cm^3 molecule^{-1} s^{-1}, both measurements at 293 K. The uncertainties in the rate constant measurements include an estimate of systematic and random errors at the 2σ confidence level. The present estimates for k_{2a} are a factor of 5 smaller than an estimate based on a detailed theoretical calculation.[9] The measurements of k_3 are in good agreement with the only previous measurement of this rate constant.[10]

Acknowledgment. This work was performed under the auspices of the Office of Basic Energy Sciences, Division of Chemical Sciences, Geosciences, and Biosciences, U.S. Department of Energy, under Contract DE-AC02-06CH11357.

References and Notes

(1) Pilling, M. J.; Stocker, D. W. *Annu. Prog. Chem., Sect. C* **1999**, *95*, 277.

(2) Holbrok, K. A.; Pilling, M. J.; Robertson, S. H. *Unimolecular Reactions*, 2nd ed.; John Wiley & Sons: Chichester, U.K., 1996.

(3) Miller, J. A.; Bowman, C. T. *Prog. Energy Combust.* **1989**, *15*, 287.

(4) Dean, A. M.; Bozzelli, J. W. In *Gas-Phase Combustion Chemistry*; Gardiner, W. C., Jr., Ed.; Springer-Verlag: New York, 1996.

(5) Huges, K. J.; Tomlin, A. S.; Hampartsoumian, E.; Nimmo, W.; Zsély, I. G.; Ujvári, M.; Turányi, T.; Claugue, A. R.; Pilling, M. J. *Combust. Flame* **2001**, *124*, 573.

(6) Davidson, D. F.; Kohse-Höinghaus, K.; Chang, A. Y.; Hanson, R. K. *Int. J. Chem. Kinet.* **1990**, *22*, 513.

(7) Rohrig, M.; Wagner, H. G. *Twenty-Fifth Symposium (International) on Combustion*; The Combustion Institute: Pittsburg, PA, 1994, p 975.
(8) Fontijin, A.; Shamsuddin, S. M.; Grammond, D.; Marshall, P.; Anderson, W. R. *Combust. Flame* **2006**, *145*, 543.
(9) Linder, D. P.; Duan, X.; Page, M. *J. Chem. Phys.* **1996**, *104*, 6298.
(10) Dransfeld, P.; Hack, H.; Kurzke, H.; Temps, F.; Wagner, H. G. *Twentieth Symposium (International) on Combustion*; The Combustion Institute: Pittsburg, PA, 1984, p 655.
(11) Ross, S. C.; Biss, F. W.; Vervloet, M.; Ramsay, D. A. *J. Mol. Spectrosc.* **1988**, *129*, 436.
(12) Bernath, P. F.; Amano, T. *J. Mol. Spectrosc.* **1982**, *95*, 359.
(13) Bahng, M.-K.; Macdonald, R. G. *J. Phys. Chem. A* **2008**, *112*, 13432–13443.
(14) He, G.; Tokue, I.; Harding, L. B.; Macdonald, R. G. *J. Phys. Chem. A* **1998**, *102*, 7653.
(15) Bahng, M.-K.; Macdonald, R. G. *J. Phys. Chem. A* **2007**, *111*, 3850.
(16) Chackerian, C., Jr.; Guelachvili, G.; López-Piñerio, A.; Tipping, R. H. *J. Chem. Phys.* **1989**, *90*, 641.
(17) Cantarella, E.; Culot, F.; Liévin, J. *Phys. Scr.* **1992**, *46*, 489.
(18) Gordon, S.; Mulac, W.; Nangia, P. *J. Phys. Chem.* **1971**, *75*, 2087.
(19) Nicholas, J. E.; Spiers, A. I.; Martin, N. A. *Plasma Chem. Plasma Proc.* **1986**, *6*, 39.
(20) Xu, Z.-F.; Fang, D.-C.; Fu, X.-Y. *Chem. Phys. Lett.* **1997**, *275*, 386.
(21) Adam, L.; Hack, W.; Zhu, H.; Qu, Z.-W.; Schinke, R. *J. Chem. Phys.* **2005**, *122*, 11430.
(22) Baulch, D. L.; Cobos, C. J.; Cox, R. A.; Esser, C.; Frank, P.; Just, Th.; Kerr, J. A.; Pilling, M. J.; Troe, J.; Walker, R. W.; Warnatz, J. *J. Phys. Chem. Ref. Data* **1992**, *21*, 411.
(23) Vaghjiani, G. L. *Int. J. Chem. Kinet.* **1995**, *27*, 777.
(24) Gehring, V. M.; Hoyermann, K.; Wagner, H.Gg.; Wolfrum, J. *Ber. Bunsen. Phys. Chem.* **1971**, *75*, 1287.
(25) Konnov, A. A.; Ruyck, J. D. *Combust. Flame* **2001**, *124*, 106.
(26) Gao, Y.; Macdonald, R. G. *J. Phys. Chem. A* **2005**, *109*, 5388.
(27) Miller, J. A.; Smooke, M. D.; Green, R. M.; Kee, R. J. *Combust. Sci. Technol.* **1983**, *34*, 149.
(28) Warnatz, J.; Maas, U.; Dibble, R. W. *Combustion: Physical and Chemical Fundamentals, Modeling and Simulation, Experiments, Pollutant Formation*, 2nd ed.; Springer: Berlin, 1995.
(29) Yamasaki, K.; Watanabe, A.; Tanaka, A.; Sato, M.; Tokue, I. *J. Phys. Chem.* **2002**, *106*, 6563.
(30) Kaes, A.; Stuhl, F. *J. Chem. Phys.* **1992**, *97*, 7362.
(31) Hake, A.; Stuhl, F. *J. Chem. Phys.* **2002**, *117*, 2513.
(32) Kenner, R. D.; Browarzik, R. K.; Stuhl, F. *Chem. Phys.* **1988**, *121*, 457.
(33) Kenner, R. D.; Rohrer, F.; Stuhl, F. *J. Chem. Phys.* **1987**, *86*, 2036.
(34) Donnelly, V. M.; Baronavski, A. P.; McDonald, J. R. *Chem. Phys.* **1979**, *43*, 271.
(35) Zetzsch, C.; Stuhl, F. *Ber. Bunsen. Phys. Chem.* **1976**, *80*, 1354.
(36) Bower, R. D.; Jacoby, M. T.; Blauer, J. A. *J. Chem. Phys.* **1987**, *86*, 1954.
(37) Piper, L. G.; Krech, R. H.; Taylor, R. L. *J. Chem. Phys.* **1980**, *73*, 791.
(38) Rohrer, F.; Stuhl, F. *Chem. Phys. Lett.* **1984**, *111*, 234.
(39) Adam, L.; Hack, W.; Olzmann, M. *Z. Phys. Chem.* **2004**, *218*, 439.
(40) Fernández-Ramos, A.; Miller, J. A.; Klippenstein, S. J.; Truhlar, D. G. *Chem. Rev.* **2006**, *106*, 4518.

JP809643U